

Effect of orientation and mode of loading on deformation behaviour of Cu nanowires

P. Rohith^a, G. Sainath^{a,*}, B.K. Choudhary^a

^a*Materials Development and Technology Division, Metallurgy and Materials Group, Indira Gandhi Centre for Atomic Research, HBNI, Kalpakkam, Tamilnadu-603102, India*

Abstract

Molecular dynamics simulations have been performed to understand the variations in deformation mechanisms of Cu nanowires as a function of orientation and loading mode (tension or compression). Cu nanowires of different crystallographic orientations distributed uniformly on the standard stereographic triangle have been considered under tensile and compressive loading. The simulation results indicate that under compressive loading, the orientations close to $\langle 100 \rangle$ corner deform by twinning mechanism, while the remaining orientations deform by dislocation slip. On the other hand, all the nanowires deform by twinning mechanism under tensile loading. Further, the orientations close to $\langle 110 \rangle$ and $\langle 111 \rangle$ corner exhibit tension-compression asymmetry in deformation mechanisms. In addition to deformation mechanisms, Cu nanowires also display tension-compression asymmetry in yield stress. The orientations close to $\langle 001 \rangle$ corner exhibits higher yield stress in tension than in compression, while the opposite behaviour (higher yield stress in compression than in tension) has been observed in orientations close to $\langle 110 \rangle$ and $\langle 111 \rangle$ corners. For the specific orientation of $\langle 102 \rangle$, the yield stress asymmetry has not been observed. The tension-compression asymmetry in deformation mechanisms has been explained based on the parameter α_M , defined as the ratio of Schmid factors for leading and trailing partial dislocations. Similarly, the asymmetry in yield stress values has been attributed to the different Schmid factor values for leading partial dislocations under tensile and compressive loading.

Keywords: Molecular Dynamics simulations, Cu nanowire, Orientation, Dislocations and Twinning

1. Introduction

In recent years, the metallic nanowires have attracted a significant interest for research due to their superior electrical, optical, thermal and mechanical properties. In particular the Cu nanowires/nanopillars, nanobelts, nanosprings and nanofilms have emerged as the next-generation materials in nano/micro electromechanical systems (NEMS/MEMS) due to their excellent performance with conductivity, transmittance, mechanical flexibility, low cost, easy and inexpensive synthesis [1, 2]. In view of this, understanding the deformation behaviour of Cu nanowires becomes essential for their effective practical applications. The knowledge

*Corresponding author
Email address: sg@igcar.gov.in (G. Sainath)

of deformation mechanisms also becomes important for fine-tuning the physical properties of nanowires such as reorientation, shape-memory and pseudo-elasticity [3], which have practical implications in the design of novel and flexible NEMS/MEMS devices.

In view of the small size of nanowires, performing the accurate mechanical testing of nanowires is still challenging due to the difficulties in sample preparation, clamping and aligning the nanowire axial direction with loading direction [4]. These complexities in experimental techniques preclude the conventional methods and lend towards theoretical/computational tools. With the rapid progress of computational capability and the availability of reliable inter-atomic potentials, molecular dynamics (MD) simulations have become a major tool to probe the mechanical properties of nanoscale materials. In addition to the usual mechanical properties, MD simulations provide the real-time deformation process of nanowire at the atomic scale. In the present study, MD simulations have been used to understand the deformation mechanisms in Cu nanowires.

In the past, many experimental/atomistic simulations have been performed on FCC nanowires/nanopillars such as Au [5, 6, 7], Ag [8], Cu [5, 9], Pt [10], Al [11] and Ni [5, 12]. All these studies have shown that the important mechanisms of plastic deformation in FCC nanowires are slip through perfect and partial dislocations and deformation twinning. The competition between slip and twinning mechanisms depends mainly on the crystallographic orientation, size, shape and loading mode (tension/compression), temperature and strain rate [13, 14, 15]. However, among all these factors, crystallographic orientation has the strongest influence followed by mode of loading [12, 13]. For example, Zheng et al. [6] studied the orientation dependent deformation behaviour of Au nanocrystals using in-situ high resolution transmission electron microscope (HRTEM) combined with MD simulations. It has been shown that under tensile loading of Au nanocrystal, the deformation by slip is favoured in $\langle 100 \rangle$ orientation, while twinning is observed in $\langle 110 \rangle$ orientation. This study further confirmed that, despite large differences in strain rates, the results obtained using MD simulations are in good agreement with experimental results [6]. Similar to $\langle 110 \rangle$ orientation, the deformation by partial slip/twinning is preferred under the tensile loading of $\langle 111 \rangle$ oriented FCC nanowires [9]. In order to understand the influence of mode of loading (tension/compression), Lee et al. [7] carried out the experimental and atomistic simulation study on the tensile and compressive deformation of $\langle 110 \rangle$ Au nanopillars. Under tensile loading, the deformation by twinning was observed, while dislocation slip has occurred under the compressive loading of $\langle 110 \rangle$ Au nanopillar [7]. Contrary to $\langle 110 \rangle$ orientation, the $\langle 100 \rangle$ oriented FCC nanowires deform by slip under tensile loading, while twinning is observed under compressive loading [5, 6, 13]. These results strongly suggest that the deformation behaviour of FCC nanowires depends on the orientation and mode of loading. However, in the literature, the deformation mechanisms and tension-compression asymmetry have been investigated mainly in high symmetry $\langle 100 \rangle$, $\langle 110 \rangle$ and $\langle 111 \rangle$ crystallographic orientations, which constitutes the corners of a standard stereographic triangle [13]. In view of this, understanding the deformation mechanisms over a wide range of orientations in FCC nanowires becomes important. Moreover, the variations of yield strength and strength asymmetry with respect orientation have not been studied systematically.

In the present study, MD simulations have been performed on Cu nanowires of different crystallographic orientations distributed uniformly on the standard stereographic triangle. The orientations falling on the corners, boundaries and in the interior of the standard stereographic triangle have been considered. In addition to above, the influence of loading mode (tension/compression) has been examined for all the orientations. The yielding behaviour, yield strength and deformation mechanisms of all the nanowires under tensile and compressive loadings have been presented. Finally an attempt has been made to understand the orientation dependent deformation mechanisms in terms of the ratio of leading partial Schmid factor to trailing partial Schmid factor.

2. MD Simulation details

Molecular dynamics (MD) simulations have been performed using Large scale Atomic/Molecular Massively Parallel Simulator (LAMMPS) package [16] employing an embedded atom method (EAM) potential for FCC Cu given by Mishin and co-workers [17]. This potential has been chosen for being able to reproduce stacking fault and twinning fault energies for Cu [18], which are key variables for predicting the dislocation nucleation and deformation mechanisms in nanowires.

In order to examine the influence of orientation on the deformation behaviour, MD simulations have been performed on Cu nanowires of different crystallographic orientations distributed uniformly over the standard stereographic triangle (Fig. 1). The orientations falling on the corners ($\langle 100 \rangle$, $\langle 110 \rangle$ and $\langle 111 \rangle$), boundaries ($\langle 115 \rangle$, $\langle 113 \rangle$, $\langle 112 \rangle$, $\langle 212 \rangle$, $\langle 102 \rangle$ and $\langle 103 \rangle$) and interior ($\langle 213 \rangle$, $\langle 214 \rangle$, $\langle 315 \rangle$ and $\langle 516 \rangle$) of the standard stereographic triangle have been considered. The side surfaces of all the nanowires with different orientations have been presented in Table 1. All the nanowires have a square cross-section width (d) of 10 nm and length of 20 nm, providing an aspect ratio of 2:1. Periodic boundary conditions have been chosen along the nanowire length direction, while the other two directions were kept free in order to mimic an infinitely long nanowire. Following initial construction of the nanowire, energy minimization was performed by conjugate gradient method to obtain a relaxed structure. The relaxed nanowire is thermally equilibrated to a required temperature of 10 K in canonical ensemble (constant NVT) with a Nose-Hoover thermostat. Velocity verlet algorithm has been used to integrate the equations of motion with a time step of 2 fs.

Upon completion of the equilibration process, the nanowires were deformed under tensile and compressive loading at a constant engineering strain rate of $1 \times 10^8 \text{ s}^{-1}$ along the nanowire length direction. The strain rate considered in MD simulations is significantly higher than the experimental strain rates, which is due to the inherent time scale limitations from molecular dynamics. The strain (ϵ) has been calculated as $(l - l_0)/l_0$, where l is instantaneous length and l_0 is the initial length of the nanowire. The stress has been obtained using the Virial expression [19], which is equivalent to a Cauchy's stress in an average sense. Finally, AtomEye package [20] and OVITO [21] have been used for the visualisation of atomic snapshots with common neighbour analysis (CNA) [22, 23].

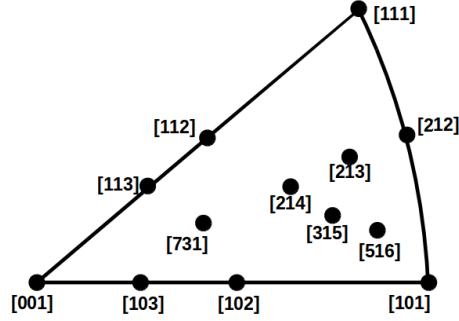


Fig. 1: Standard stereographic triangle showing the different orientations considered in this study. Cu nanowires with these orientations have been subjected to tensile and compressive loading.

Table 1: The nanowire orientations along with their side surfaces.

Orientation	$\langle 001 \rangle$	$\langle 101 \rangle$	$\langle 102 \rangle$	$\langle 103 \rangle$	$\langle 111 \rangle$	$\langle 112 \rangle$	$\langle 113 \rangle$	$\langle 212 \rangle$	$\langle 213 \rangle$	$\langle 214 \rangle$	$\langle 315 \rangle$	$\langle 516 \rangle$
Side surfaces	{100}	{100}	{100}	{100}	{110}	{110}	{110}	{110}	{111}	{201}	{130}	{111}
	{100}	{110}	{120}	{130}	{112}	{111}	{233}	{114}	{145}	{1,2,10}	{123}	{4,7,11}

3. Results

3.1. Deformation behaviour under compression

The compressive loading has been performed on Cu nanowires of different crystallographic orientations up to a strain value of 0.4. The evolution of atomic configurations at various stages of deformation were analysed for all the orientations using the common neighbour analysis. Based on this analysis, the deformation mechanisms under the compressive loading of Cu nanowires have been classified into twinning and dislocation slip as described in the following:

3.1.1. Deformation through twinning

Cu nanowires with $\langle 100 \rangle$, $\langle 103 \rangle$ and $\langle 113 \rangle$ orientations (Fig. 1) deforms by twinning mechanism under compressive loading. As a representative of twinning mechanism, Fig. 2 shows the deformation behaviour of $\langle 100 \rangle$ Cu nanowire at different strain levels. It can be seen that the nanowire yields through the nucleation of a single $1/6\langle 112 \rangle$ Shockley partial dislocation on $\{111\}$ plane from the corner with a stacking fault in its wake (Fig. 2a). On the contrary, nucleation of multiple Shockley partial dislocations has been observed during the compressive deformation of $\langle 103 \rangle$ and $\langle 113 \rangle$ Cu nanowires. Following yielding, another Shockley partial nucleates on the adjacent plane and creates micro-twin in the nanowire (Fig. 2b). This shows that the presence of stacking faults are must for formation of twins in the nanowires [24, 25]. The stacking faults needed to form the twins were created by the glide of leading partials nucleated from the nanowire surface. With increasing strain, the continuous nucleation and glide of twinning partials along the twin boundaries leads to twin growth (Fig. 2c). It can be seen that the twinning partials glide in mutually opposite directions on two twin boundaries and as a result the twin boundaries move away from each other leading to the twin growth (Fig. 2c). The continuous propagation of twin boundaries along the nanowire

length progressively reorients the twinned region. Due to periodic boundary conditions along the nanowire length, the twin boundaries across the length meet each other and annihilate leaving a defect free reoriented nanowire (Fig. 2d). Thus, the deformation by twinning on a single twin system transforms the orientation of nanowire from $\langle 100 \rangle / \{100\}$ to $\langle 110 \rangle / \{111\}$. After the reorientation, the nanowire again undergoes an elastic deformation followed by yielding through the nucleation of a new $1/6\langle 112 \rangle$ Shockley partial on a different crystallographic plane. Following yielding, the deformation in the reoriented nanowire proceeds by the slip of extended dislocations (Fig. 2e). Similar to $\langle 100 \rangle$ nanowire, deformation by partial slip and twinning has been observed under the compressive loading of $\langle 103 \rangle$ and $\langle 113 \rangle$ Cu nanowires. However, due to twin-twin interactions, the reorientation has not been observed in $\langle 103 \rangle$ and $\langle 113 \rangle$ nanowires.

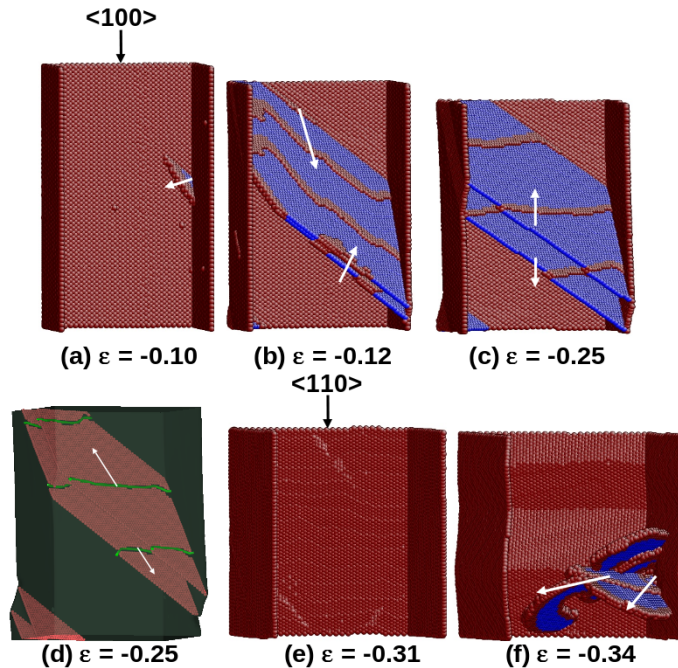


Fig. 2: Atomic snapshots displaying (a) nucleation of a Shockley partial, (b) glide of twinning partial and micro-twin, (c-d) twin growth (e) reoriented nanowire, and (f) the slip of extended dislocation in the reoriented nanowire during the compressive deformation of $\langle 100 \rangle$ Cu nanowires. In Figure (d), the partial dislocations are shown as green lines as obtained in OVITO, while the remaining figures are obtained using AtomEye. The atoms are coloured according to the common neighbour analysis (CNA). The blue colour atoms represents the FCC and the red colour atoms indicate the surfaces and dislocation core.

3.1.2. Deformation through slip

The Cu nanowires with $\langle 101 \rangle$, $\langle 111 \rangle$, $\langle 102 \rangle$, $\langle 212 \rangle$, $\langle 213 \rangle$, $\langle 214 \rangle$, $\langle 315 \rangle$ and $\langle 516 \rangle$ orientations deform by full dislocation slip mechanism. As an example, the deformation behaviour in $\langle 111 \rangle$ (representing the orientations along the boundary of a triangle in Fig. 1) and $\langle 214 \rangle$ (representing the orientations inside the triangle in Fig. 1) Cu nanowires has been presented in Fig. 3 and 4, respectively. It can be seen that the yielding in both the nanowires occurs through the nucleation of a leading partial immediately followed by trailing partial, thus constituting an extended dislocation (Fig. 3a and 4a). However in $\langle 111 \rangle$ nanowire, the activation of many slip planes has been observed, while in $\langle 214 \rangle$ nanowire, the activation of only two

slip systems has been observed. Following yielding, the nucleated dislocations glide from one corner of the nanowire to the opposite and gets annihilated by leaving a slip steps on the surface of the nanowire (Figs. 3b and 4b). The activation of different slip systems in $\langle 111 \rangle$ nanowire facilitates dislocation-dislocation interactions, which results in the formation of many point defects and also the stacking fault tetrahedron as shown in Fig. 3b-c. Due to the activation of limited slip system in $\langle 214 \rangle$ nanowire, the formation of point defects has not been observed in the strain range examined (Fig. 4b-c). Generally, the stacking fault tetrahedron (SFT) in low stacking fault energy materials can form through vacancy condensation, or by an extension of Frank partial dislocation loop or through dislocation-dislocation interactions. However, the SFT formation through vacancy condensation requires longer time scales, which are difficult to access using MD simulations. In the present study, the SFTs have been formed through dislocation-dislocation interactions, similar to that observed by Wang et al. [26].

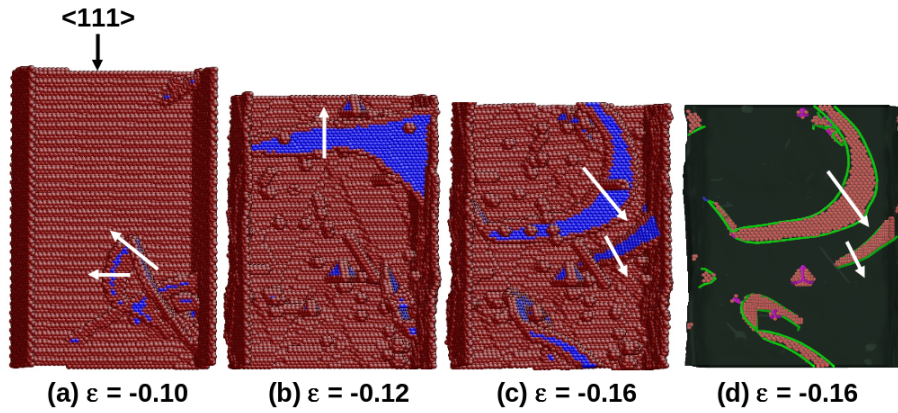


Fig. 3: Atomic snapshots displaying the compressive deformation of $\langle 111 \rangle$ Cu nanowires as a function of strain. The deformation by the slip of extended dislocations along with stacking fault tetrahedron and many point defects can be seen in (b), (c) and (d). Figure (d) is the OVITO output of Figure (c), where partial dislocations are shown as green lines, the stair-rod dislocations enclosing the stacking fault tetrahedron are shown in magenta lines. The atoms are coloured according to the common neighbour analysis (CNA).

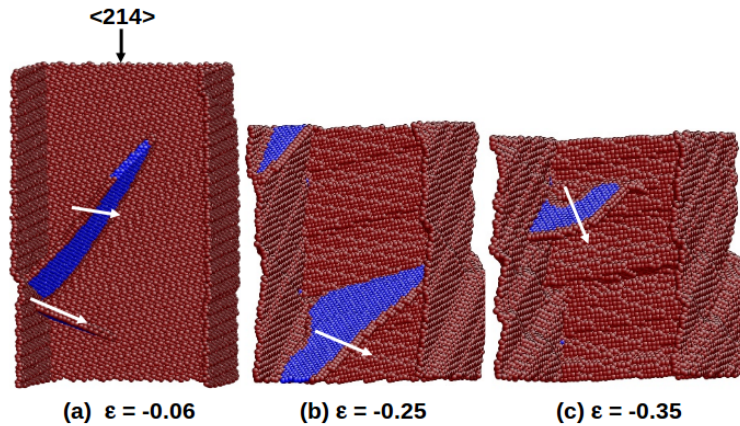


Fig. 4: Atomic snapshots displaying the compressive deformation of $\langle 214 \rangle$ Cu nanowires as a function of strain. The deformation proceeds through the glide of extended dislocations. The atoms are coloured according to the common neighbour analysis (CNA).

3.2. Deformation behaviour under tension

In order to investigate the influence of loading mode on the deformation behaviour, MD simulations have been performed on the tensile loading of Cu nanowires with different orientations shown in Fig. 1. It has been observed that under tensile loading, the deformation in all the Cu nanowires is dominated by twinning mechanism irrespective of the orientations. Full dislocation slip has not been observed in any of the orientations examined. Further, it has been observed that the twinning in certain orientations leads to complete reorientation of the nanowires, while in remaining orientations, it leads to neck formation and early failure without any reorientation. Therefore, the tensile deformation of Cu nanowires has been classified into (i) twinning leading to full reorientation of the nanowire and (ii) twinning without full reorientation.

3.2.1. Twinning leading to full reorientation of the nanowire

Twinning under tensile loading of $\langle 101 \rangle$, $\langle 103 \rangle$, $\langle 212 \rangle$ and $\langle 214 \rangle$ orientations leads to complete reorientation of the nanowires. As an example, the deformation by twinning followed by reorientation in $\langle 101 \rangle$ and $\langle 214 \rangle$ nanowires has been presented in Figs. 5 and 6, respectively. It can be seen that the yielding in both the orientations occurs by the nucleation of Shockley partial dislocations (Figs. 5a and 6a). However in $\langle 101 \rangle$ nanowire, the activation of two different slip planes has been observed (Fig. 5a), while in $\langle 214 \rangle$ nanowire, the activation of only one slip system can be seen in Fig. 6a. Following the nucleation of Shockley partials during yielding, the subsequent nucleation of twinning partial dislocations leads to the formation of twins on the corresponding $\{111\}$ planes (Figs. 5b and 6b). With increasing strain, the twin grows along the nanowire axis leading to complete reorientation of nanowires (Figs. 5c and 6c). Due to twinning, the $\langle 101 \rangle$ nanowire reorients to $\langle 100 \rangle$ nanowire, while $\langle 214 \rangle$ nanowire reorients to a high indexed $\langle hkl \rangle$ direction. Generally, the reorientation is not observed when the slip is activated on more than one twin system, due to twin-twin interactions. However, the $\langle 101 \rangle$ nanowire undergoes reorientation despite the activation of multiple twin systems (Fig. 5a-c). Following the reorientation, the nanowires undergo a second elastic deformation followed by yielding through the nucleation of Shockley partial dislocations (Figs. 5d and 6d). Following the second yielding in $\langle 101 \rangle$ nanowire, twin formation and the interaction of twin boundaries with Shockley partial dislocations results in neck formation and final failure as shown in Fig. 5e. On the contrary, the sliding along the twin boundaries (Fig. 6e) leading to shear failure (Fig. 6f) accompanied with large strain to failure has been observed in $\langle 214 \rangle$ nanowire.

3.2.2. Twinning without full reorientation

Unlike the $\langle 101 \rangle$, $\langle 103 \rangle$, $\langle 212 \rangle$ and $\langle 214 \rangle$ orientations, the twinning in $\langle 100 \rangle$, $\langle 102 \rangle$, $\langle 111 \rangle$, $\langle 112 \rangle$ and $\langle 113 \rangle$ orientations doesn't lead to reorientation. Generally, when the slip is activated on more than one twin system, there is an increased probability of twin-twin interactions, which disrupts the twin growth process and reorientation [27]. Similarly, when the sliding along the twin boundaries is preferred over twin boundary migration (which is necessary for twin growth), the reorientation is not observed. As an example, the twin-twin interactions and the twin boundary sliding disrupting the reorientation process in

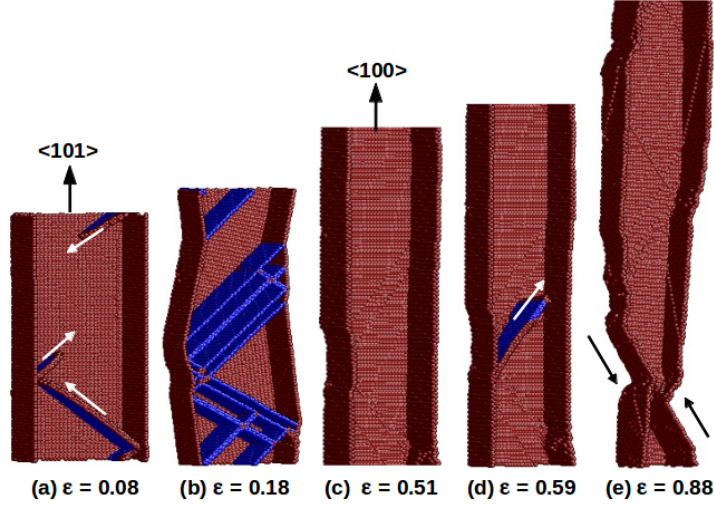


Fig. 5: The atomic snapshots displaying the tensile deformation of $\langle 110 \rangle$ Cu nanowires as a function of strain. Deformation proceeds through twinning followed by reorientation to $\langle 100 \rangle$ axial direction.

$\langle 100 \rangle$ and $\langle 102 \rangle$ Cu nanowires has been demonstrated in Fig. 7. In $\langle 100 \rangle$ nanowire, the twin boundary sliding dominates over twin growth (Fig. 7a-b), thus making the nanowire to show shear failure without reorientation. On the other hand in $\langle 102 \rangle$ nanowire, the slip-twin interactions along with the sliding of twin boundaries were responsible for the absence of reorientation (Fig. 7c-d).

3.3. Stress-strain behaviour

Figure 8 shows the stress-strain behaviour of Cu nanowires of different orientations under compressive loading. It can be seen that initially all the nanowires undergo elastic deformation up to a peak value followed by an abrupt drop in flow stress. Following the yield drop, the flow stress fluctuates about a constant mean value. In nanowires deforming by twinning mechanism, marginal fluctuations have been observed about a mean value of 1.3 GPa for $\langle 100 \rangle$ nanowire and 2.2 GPa for $\langle 103 \rangle$ nanowire (Fig. 8a). Following this fluctuations about a mean value, $\langle 100 \rangle$ nanowire shows second large peak in the stress-strain curve, which is due to the twinning induced reorientation (Fig. 8a). On the other hand in nanowires deforming by full dislocation slip, the flow stress shows large fluctuations about a constant mean value of 3 GPa irrespective of the nanowire orientation (Fig. 8b).

Figure 9 shows the stress-strain behaviour of Cu nanowires with different orientations under tensile loading. It can be seen that the stress-strain behaviour of nanowires undergoing a twinning induced reorientation (Fig. 9a) is different from that of the nanowires not showing the reorientation (Fig. 9b). During plastic deformation of nanowires not showing reorientation, the flow stress decreases continuously till failure (Fig. 9b), while the flow stress in nanowires undergoing reorientation exhibits a “U” shape behaviour (Fig. 9a), where the second peak corresponds to the elastic deformation of the reoriented nanowires. Following the second peak, the flow stress decreases continuously till failure, similar to the nanowires not showing reorien-

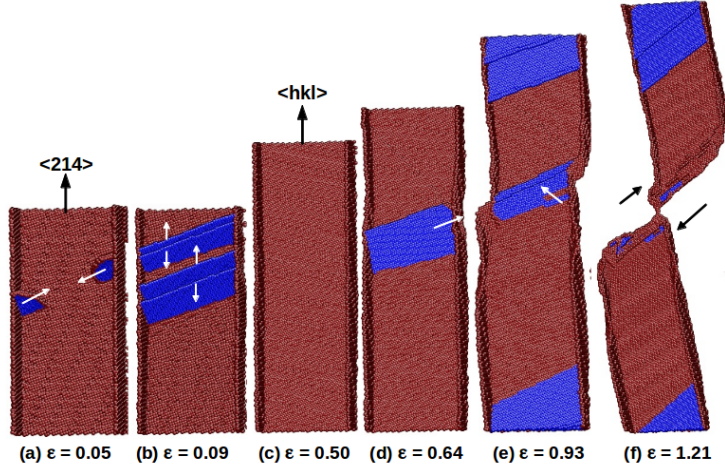


Fig. 6: The atomic snapshots during the tensile deformation of $\langle 214 \rangle$ Cu nanowires as a function of strain. Deformation proceeds through twinning mechanism followed by reorientation to high index $\langle hkl \rangle$ direction. The final failure occurs by sliding along the twin boundaries.

tation. Despite similar deformation mechanism by twinning, large variations in strain failure can be seen in Cu nanowires of different orientations under tensile loading.

Following the yielding, the peak value in the stress-strain curve has been taken as the yield stress for Cu nanowires of different orientations and presented on the standard stereographic triangle under compressive and tensile loading as shown in Fig. 10. Under compressive loading, it can be seen that the Cu nanowires with orientation close to $\langle 001 \rangle$ corner display the low values of yield stress (Fig. 10a). As the orientations move away from the $\langle 001 \rangle$ corner, an increase in compressive yield stress can be seen. The $\langle 111 \rangle$ and $\langle 101 \rangle$ oriented nanowires display the highest compressive yield stress values of 20.2 GPa and 13.1 GPa, respectively (Fig. 10a). Contrary to compressive loading, the orientations close to $\langle 101 \rangle$ corner display the low values of yield stress under tensile loading (Fig. 10b). As the orientations move towards $\langle 111 \rangle$ and $\langle 001 \rangle$ corners, an increase in tensile yield stress can be seen in Fig. 10b. Under tensile loading, the $\langle 111 \rangle$ and $\langle 001 \rangle$ oriented nanowires exhibits the highest values of yield stress. It is interesting to note that the $\langle 111 \rangle$ oriented Cu nanowires display the highest value of yield stress under both tensile and compressive loading.

4. Discussion

4.1. Orientation and loading mode dependent deformation mechanisms

MD simulation results indicate that under compressive loading, the $\langle 100 \rangle$, $\langle 103 \rangle$ and $\langle 113 \rangle$ oriented Cu nanowires deform by twinning mechanism, while the remaining orientations deform by dislocation slip. On the other hand all the nanowires deform by twinning mechanism under tensile loading. Full dislocation slip has not been observed in any of the orientations under tensile loading. The deformation by twinning in certain orientations has lead to the complete reorientation of the nanowires. These results shows that the $\langle 100 \rangle$,

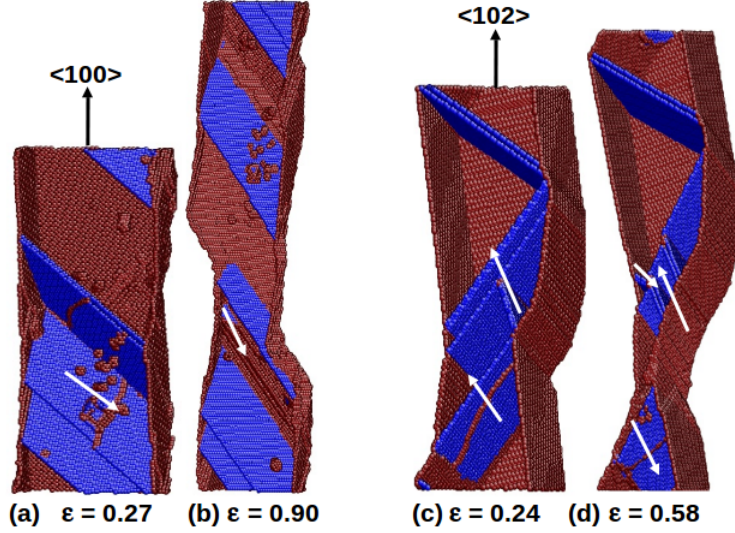


Fig. 7: Atomic snapshots presenting the deformation and failure behaviour of $\langle 100 \rangle$ and $\langle 102 \rangle$ Cu nanowires under tensile loading. The twin-twin interactions and the twin boundary sliding disrupting the reorientation process can be seen in both the orientations.

$\langle 103 \rangle$ and $\langle 113 \rangle$ Cu nanowires deform by twinning mechanism, irrespective of the loading modes of tension and compression. Cu nanowires with remaining orientations exhibit tension-compression asymmetry in deformation mechanisms in terms of full dislocation slip under compressive loading and twinning under tensile loading. In the past, the tension-compression asymmetry in deformation mechanisms has been revealed in BCC nanowires [34] and also in high symmetry $\langle 110 \rangle$ and $\langle 111 \rangle$ oriented FCC nanowires [5, 7]. However, the present study shows that the asymmetry in deformation mechanisms of FCC nanowires is not limited to $\langle 110 \rangle$ or $\langle 111 \rangle$ orientations, but it exists in many other orientations close to $\langle 110 \rangle$ and $\langle 111 \rangle$ corners of the standard stereographic triangle.

The orientation and mode of loading dependent deformation behaviour of FCC nanowires can be understood based on the Schmid factor (m) analysis [5, 13]. According to this analysis, if the Schmid factor of leading partial is higher than the trailing partial, then the deformation proceeds by the slip of partial dislocations or twinning [13]. On the other hand, if the Schmid factor of trailing partials is higher than the leading partials, nucleation of trailing partial immediately follows the already nucleated leading partial and this results in deformation dominated by the slip of full or extended dislocations [13]. The Schmid factor values for leading (m_L) and trailing (m_T) partials for some of the orientations of Cu nanowires along with the predicted and observed deformation mechanisms are presented in Table 2. It can be seen that for most of the orientations, the predicted mechanisms using the Schmid factor analysis are in good agreement with the observed mechanisms in the present study. The exception is being the $\langle 100 \rangle$, $\langle 103 \rangle$ and $\langle 113 \rangle$ orientations under tensile loading. This exception can arise from the effects associated with the orientation of the side surfaces and also the nanowire size, which are not considered in the Schmid factor calculations [5, 13, 28]. When the nanowire is enclosed by high energy side surfaces, it tries to minimize the surface energy by reorienting the surfaces, which is possible only when the deformation proceeds by twinning mech-

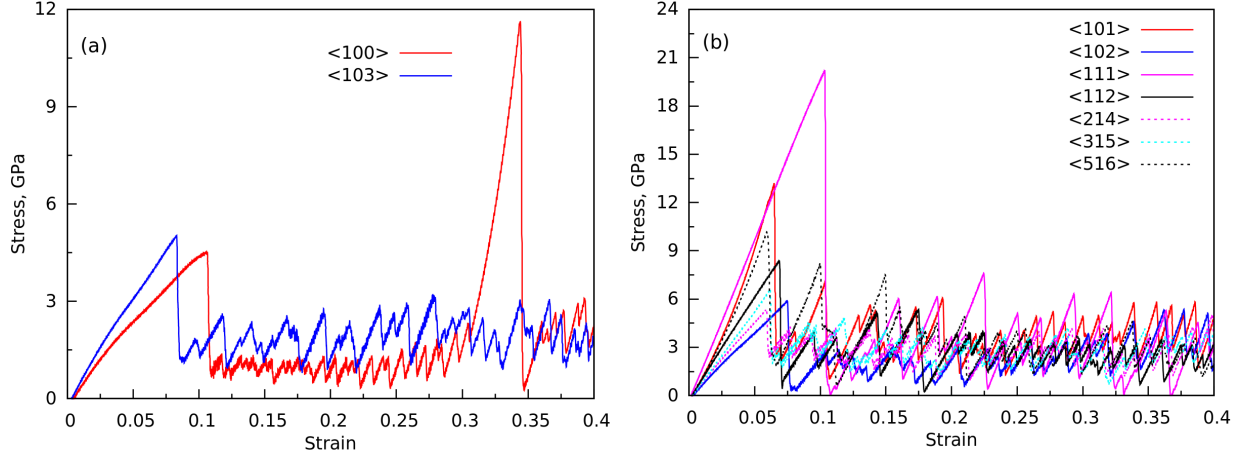


Fig. 8: The stress-strain behaviour of Cu nanowires deforming by (a) twinning and (b) full dislocation slip under compressive loading of different orientations at 10 K.

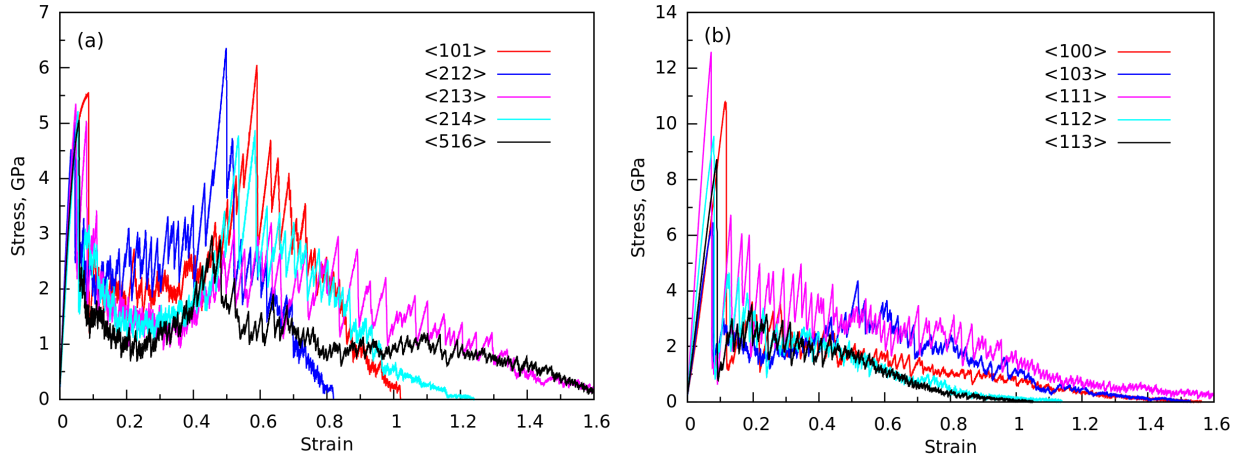


Fig. 9: The stress-strain behaviour of Cu nanowires deforming by twinning (a) with reorientation and (b) without reorientation under tensile loading at 10 K.

anism. Therefore in nanowire with high energy side surfaces generally twinning is preferred over dislocation slip, even though Schmid factor predicts otherwise. Similarly in small size nanowires partial slip/twinning is preferred, while increasing the size above certain value changes the deformation mode from twinning to full dislocation slip as reported in the previous study on $\langle 100 \rangle$ Cu nanowires [28, 29].

The above mentioned Schmid factor analysis can be generalized for all the orientations in standard stereographic triangle by defining a parameter α_M , as the ratio of Schmid factors for leading and trailing partial dislocations (Table 2). The values of α_M for different orientations of Cu nanowires have been shown on standard stereographic triangle in Figs. 11a and b under compressive and tensile loading, respectively. Based on the values of α_M , the orientations in the triangle can be divided into two regions, one with $\alpha_M > 1$ and the other with $\alpha_M < 1$, separated by a boundary line with $\alpha_M = 1$. It can be seen that for the region where $\alpha_M > 1$, the Schmid factor for leading partial is higher than the trailing partials irrespective of the loading mode and as a result, the deformation by twinning/partial dislocation slip is favoured in

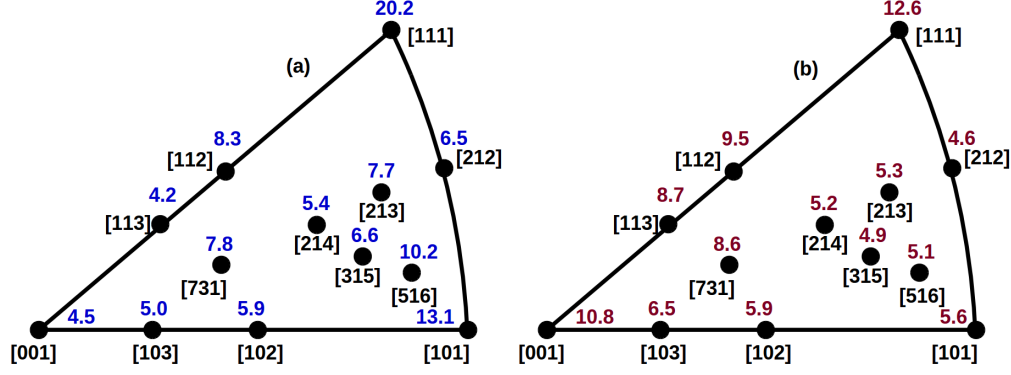


Fig. 10: The variation of yield stress with respect to orientation presented on the standard stereographic triangle under (a) compressive loading, and (b) tensile loading of Cu nanowires. The yield stress values are in GPa.

orientations falling in this region. In contrast, for the region where $\alpha_M < 1$, the Schmid factor for trailing partial dislocations is higher than the leading partials. As a consequence, the deformation by full/extended dislocations is favoured in this region. For the orientations falling on the boundary with $\alpha_M = 1$, both leading and trailing partials have equal Schmid factor values (e.g. $\langle 102 \rangle$ orientation in Table 2) and the deformation can proceed either through twinning or extended dislocations or by the combination of these two [30]. Therefore, if the nanowire orientation falls in the region with $\alpha_M > 1$, the deformation by twinning is preferred, while full dislocation slip is preferred if the orientation falls in the region with $\alpha_M < 1$. If it falls on the boundary line with $\alpha_M = 1$, both the mechanisms are equally probable [31]. The generalization of Schmid factor analysis based on the parameter α_M has an advantage as this method predicts the operative deformation mechanism in some arbitrary orientation simply based on its position on the triangle and loading mode.

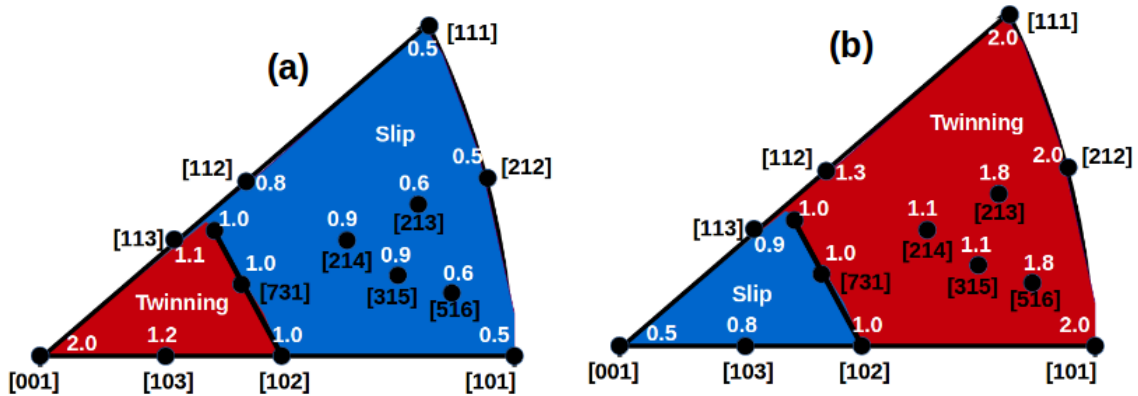


Fig. 11: The standard stereographic triangle showing two different regions, one with $\alpha_M > 1$ (red colour) and other with $\alpha_M < 1$ (light blue) under (a) compressive loading and (b) tensile loading. The black solid line between red and blue colours represent a boundary with $\alpha_M = 1$. The parameter, α_M is defined as the ratio of Schmid factors of leading and trailing partial dislocations.

Table 2: Schmid factor values for leading (m_L) and trailing (m_T) partial dislocations for some of the orientations of Cu nanowires along with the predicted and observed deformation mechanisms. The ratio of leading partial Schmid factor (m_L) to trailing partial Schmid factor (m_T) has been presented as α_M .

Nanowire orientation	Loading type	m_L	m_T	Predicted mechanism	Observed mechanism	$\alpha_M = m_L/m_T$
<100>	Tension	0.235	0.470	Full slip	Twinning	0.5
	Compression	0.470	0.235	Twinning/partial slip	Twinning	2.0
<102>	Tension	0.42	0.42	Full slip and Twinning	Twinning	1.0
	Compression	0.42	0.42	Full slip and Twinning	Full slip	1.0
<103>	Tension	0.38	0.47	Full slip	Twinning	0.8
	Compression	0.47	0.38	Twinning	Twinning	1.2
<110> & <212>	Tension	0.470	0.235	Twinning/partial slip	Twinning	2.0
	Compression	0.235	0.470	Full slip	Full slip	0.5
<111>	Tension	0.31	0.155	Twinning/partial slip	Twinning	2.0
	Compression	0.155	0.31	Full slip	Full slip	0.5
<112>	Tension	0.39	0.31	Twinning/partial slip	Twinning	1.3
	Compression	0.31	0.39	Full slip	Full slip	0.8
<113>	Tension	0.39	0.43	Full slip	Twinning	0.9
	Compression	0.43	0.39	Twinning	Twinning	1.1
<214>	Tension	0.44	0.39	Twinning/partial slip	Twinning	1.1
	Compression	0.39	0.44	Full slip	Full slip	0.9

4.2. Tension-compression asymmetry in yield stress

MD simulations results indicate that for most of the orientations, the values of yield stress were different under tensile and compressive loading i.e. the nanowires exhibit tension-compression asymmetry in yield stress. This asymmetry (r) can be better understood by considering the ratio of yield stress in tension to that in compression (T/C). Fig. 12a shows the values of asymmetry factor 'r' for different orientations on the standard stereographic triangle. It can be seen that, the asymmetry values falls in the range 0.4-2.4 and for the orientations near <001> corner, the asymmetry values are higher than the values for the orientations close to <110> and <111> corners. This suggest that, the orientations close to <001> corner exhibits higher yield stress in tension than in compression, while the opposite behaviour (higher yield stress in compression than in tension) is observed in orientations close to <110> and <111> corners. Similar to the present study, the tension-compression asymmetry in yield strength has been observed in many FCC and BCC nanowires [7, 5, 34, 32, 33]. However, the present results shows that for the specific orientation of <102>, the values of yield stress under tensile and compressive loadings have been observed to be the same, thus indicating the absence of asymmetry. In order to understand this asymmetry in yield strength, different explanations have been given in literature [32]. Weinberger et al. [32] have pointed out that the presence of tensile surface stresses is responsible for the asymmetry in yield stress of FCC nanowires. The surface stress, which is generally tensile in nature, induces a compressive stress in the nanowires and makes them stronger in tension and weaker in compression [32]. However, the present results show that this explanation may not be valid for the orientations close to <110> and <111> corners. Further, the tension- compression asymmetry

has been reported in FCC bulk single crystals, where there is no presence of surface stresses [35, 36, 37]. In the absence of surface stresses, it has been proposed that the stress normal to the slip direction and also the atomic stacking of the $\{111\}$ slip planes, which is not symmetrical about the $\langle 110 \rangle$ slip direction were responsible for the tension-compression asymmetry in FCC single crystals [35, 36, 37].

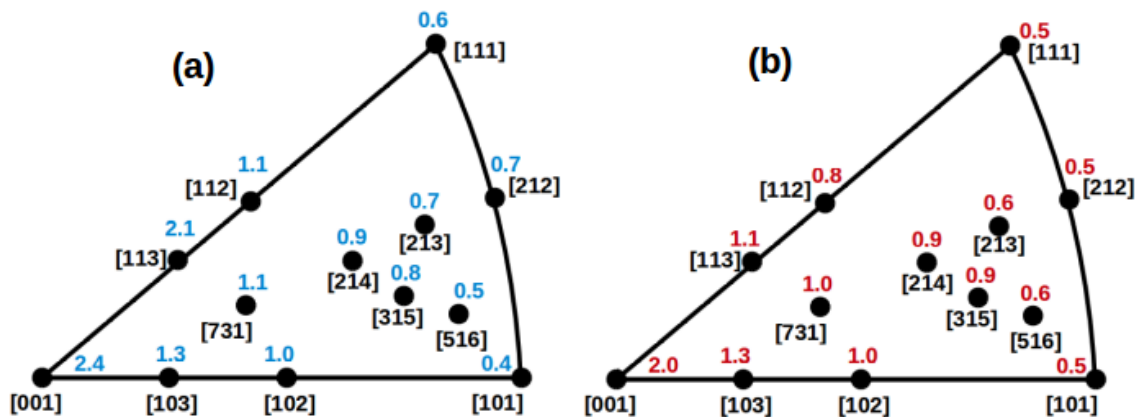


Fig. 12: The values of (a) yield stress asymmetry (b) Schmid factor asymmetry shown on the standard stereographic graphic triangle for different orientations of Cu nanowires. Yield stress asymmetry is defined as the ratio of yield stress in tension to that in compression (T/C), while the Schmid factor asymmetry is defined as the ratio of leading partial Schmid factor in compression to that in tension (C/T).

Different from the previous studies, the tension-compression asymmetry in FCC nanowires can be explained based on the Schmid factors of leading partial dislocations, which are different under tensile and compressive loading. Here, the Schmid factors of only leading partials is necessary because irrespective of the deformation mechanism (full slip/ partial slip/twinning), the first pop-in event during yielding is the nucleation of leading partial dislocation. Therefore, the yield stress is controlled mainly by the Schmid factor of leading partial dislocations. In order to relate the observed yield stress asymmetry (r) to Schmid factors of leading partials, the ratio of leading partial Schmid factor in compression to that in tension (C/T) has been taken as the Schmid factor asymmetry (s). Fig. 12b shows the values of Schmid factor asymmetry (s) for different orientations on the standard stereographic triangle. It can be seen that for most of the orientations, the values of Schmid factor asymmetry (s) were approximately close to the values of yield stress asymmetry i.e. there is one to one correlation between yield stress asymmetry and Schmid factor asymmetry (Figs. 12a and b). This correlation suggests that the asymmetry in yield stress of nanowires is arising mainly due to the different Schmid factors for leading partial dislocation under tensile and compressive loading.

5. Conclusions

Molecular dynamics simulation results have shown that the deformation mechanisms in Cu nanowires vary significantly with crystallographic orientation and mode of loading. Under compressive loading, the orientations close to $\langle 100 \rangle$ corner of a standard stereographic triangle i.e. $\langle 100 \rangle$, $\langle 103 \rangle$ and $\langle 113 \rangle$ orientations deformed by twinning mechanism, while the remaining orientations deformed by full dislocation

slip. On the other hand, all the orientations irrespective of their position on the stereographic triangle deformed by twinning mechanism under tensile loading. Further, the orientations close to $\langle 110 \rangle$ and $\langle 111 \rangle$ corners exhibited asymmetry in deformation mechanisms in terms of full dislocation slip under compressive loading and twinning under tensile loading. Irrespective of twinning or full dislocations, the orientations falling in the interior of the standard stereographic triangle deformed on a single slip/twin system, while the orientations falling on the border deformed on multiple slip/twin systems. In addition to deformation mechanisms, it has been observed that the Cu nanowires display tension-compression asymmetry in yield stress. The orientations close to $\langle 001 \rangle$ corner exhibits higher yield stress in tension than in compression, while higher yield stress in compression than in tension has been observed in orientations close to $\langle 110 \rangle$ and $\langle 111 \rangle$ corners. Interestingly, for the specific orientation of $\langle 102 \rangle$, the values of yield stress under tensile and compressive loading were found to be same, thus indicating the absence of yield stress asymmetry in $\langle 102 \rangle$ Cu nanowire. Irrespective of loading mode, the $\langle 111 \rangle$ oriented Cu nanowires displayed the highest yield stress among all the orientations investigated. The tension-compression asymmetry in deformation mechanisms has been explained based on the parameter α_M , defined as the ratio of Schmid factors for leading and trailing partial dislocations. For the nanowire orientations falling in the region with $\alpha_M > 1$, the deformation by twinning is preferred, while full dislocation slip is observed for the orientations falling in the region with $\alpha_M < 1$. For the orientations falling on the boundary line with $\alpha_M = 1$, both the mechanisms are equally probable. However, the exception is being the $\langle 100 \rangle$, $\langle 103 \rangle$ and $\langle 113 \rangle$ orientations under tensile loading, where twinning has been observed under tensile and compressive loading. Similarly, the asymmetry in yield values has been attributed to the different Schmid factor values for leading partial dislocations under tensile and compressive loading.

References

References

- [1] C. M. Lieber, Nanoscale science and technology: Building a big future from small things, MRS Bull. 28 (2003) 486-491.
- [2] <https://technology.nasa.gov/patent/TOP2-163>.
- [3] H.S. Park, K. Gall, J.A. Zimmerman, Shape memory and pseudoelasticity in metal nanowires, Phys. Rev. Lett. 95 (2005) 255504.
- [4] Y. Chen, X. An, X. Liao, Mechanical behaviors of nanowires, Appl. Phys. Rev. 4 (2017) 031104.
- [5] H.S. Park, K. Gall, J.A. Zimmerman, Deformation of FCC nanowires by twinning and slip, J. Mech. Phys. Solids 54 (2006) 1862-81.
- [6] H. Zheng, A. Cao, C.R. Weinberger, J.Y. Huang, K. Du, J. Wang, Y. Ma, Y. Xia, S.X. Mao, Discrete plasticity in sub-10 nm sized gold crystals, Nature Comm. 1 (2010) 144.

- [7] S. Lee, J. Im, Y. Yoo, E. Bitzek, D. Kiener, G. Richter, B. Kim, S.H. Oh, Reversible cyclic deformation mechanism of gold nanowires by twinning-detwinning transition evidenced from in situ TEM, *Nature Comm.* 5 (2014) 3033.
- [8] H.S. Park, C. Ji, On the thermomechanical deformation of silver shape memory nanowires, *Acta Mater.* 54 (2006) 2645-2654.
- [9] A. Cao, E. Ma, Sample shape and temperature strongly influence the yield strength of metallic nanopillars, *Acta Mater.* 56 (2008) 4816-4828.
- [10] X.W. Gu, C.N. Loynachan, Z. Wu, Y.W. Zhang, D.J. Srolovitz, J.R. Greer, Size-dependent deformation of nanocrystalline Pt nanopillars, *Nano Lett.* 12 (2012) 6385-6392.
- [11] S. Xu, Y.F. Guo, A.H.W. Ngan, A molecular dynamics study on the orientation, size, and dislocation confinement effects on the plastic deformation of Al nanopillars, *Inter. J. Plast.* 43 (2013) 116-127.
- [12] M.F. Horstemeyer, M.I. Baskes, A. Godfrey, D.A. Hughes, A large deformation atomistic study examining crystal orientation effects on the stress-strain relationship, *Inter. J. Plast.* 18 (2002) 203-229.
- [13] C.R. Weinberger, W. Cai, Plasticity of metal nanowires, *J. Mater. Chem.* 22 (2012) 3277-3292.
- [14] J. Wang, S.X. Mao, Atomistic perspective on in situ nanomechanics, *Extr. Mech. Lett.* 8 (2016) 127-139.
- [15] H. Xie, F. Yin, T. Yu, G. Lu, Y. Zhang, A new strain-rate-induced deformation mechanism of Cu nanowire: Transition from dislocation nucleation to phase transformation, *Acta Mater.* 85 (2015) 191-198.
- [16] S. Plimpton, Fast parallel algorithms for short-range molecular dynamics, *J. Comp. Phy.* 117 (1995) 1-19.
- [17] Y. Mishin, M.J. Mehl, D.A. Papaconstantopoulos, A.F. Voter, J.D. Kress, Structural stability and lattice defects in copper: Ab initio, tight-binding, and embedded-atom calculations, *Phys. Rev. B*, 63 (2001) 1-16.
- [18] W. Liang, M. Zhou, Atomistic simulations reveal shape memory of fcc metal nanowires, *Phys. Rev. B* 73 (2006) 115409.
- [19] J.A. Zimmerman, E.B. Webb, J.J. Hoyt, R.E. Jones, P.A. Klein, D.J. Bammann, Calculation of stress in atomistic simulations, *Modell. Simul. Mater. Sci. Eng.* 12 (2003) S319-S332.
- [20] J. Li, AtomEye: an efficient atomistic configuration viewer, *Modell. Simul. Mater. Sci. Eng.* 11 (2003) 173.
- [21] A. Stukowski, Visualization and analysis of atomistic simulation data with OVITO-the Open Visualization Tool, *Modell. Simul. Mater. Sci. Eng.* 18 (2010) 015012.
- [22] D. Faken, H. Jonsson, Systematic analysis of local atomic structure combined with 3D computer graphics, *Comp. Mater. Sci.* 2 (1994) 279-286.
- [23] H. Tsuzuki, P.S. Branicio, J.P. Rino, Structural characterization of deformed crystals by analysis of common atomic neighborhood, *Comp. Phy. Comm.* 177 (2007) 518-523.

- [24] A. Kardani, A. Montazeri, Temperature-based plastic deformation mechanism of Cu/Ag nanocomposites: A molecular dynamics study, *Comput. Mater. Sci.* 144 (2018) 223-231.
- [25] A. Kardani, A. Montazeri, MD-based characterization of plastic deformation in Cu/Ag nanocomposites via dislocation extraction analysis: Effects of nanosized surface porosities and voids, *Comput. Mater. Sci.* 152 (2018) 381-392.
- [26] J.W. Wang, S. Narayanan, J.Y. Huang, Z. Zhang, T. Zhu, S.X. Mao, Atomic-scale dynamic process of deformation-induced stacking fault tetrahedra in gold nanocrystals, *Nat. Commun.* 4 (2013) 2340.
- [27] G. Sainath, B.K. Choudhary, T. Jayakumar, Molecular dynamics simulation studies on the size dependent tensile deformation and fracture behaviour of body centred cubic iron nanowires, *Comp. Mater. Sci.* 104 (2015) 76-83.
- [28] G. Sainath, P. Rohith, B.K. Choudhary, Size dependent deformation behaviour and dislocation mechanisms in $\langle 100 \rangle$ Cu nanowires, *Philos. Mag.* 97 (2017) 2632-2657.
- [29] Y. Yue, P. Liu, Q. Deng, E. Ma, Z. Zhang, X. Han, Quantitative evidence of crossover toward partial dislocation mediated plasticity in copper single crystalline nanowires, *Nano Lett.* 12 (2012) 4045-4049.
- [30] Z.J. Wang, Q.J. Li, Y. Li, L.C. Huang, L. Lu, M. Dao, J. Li, S. Suresh, Z.W. Shan, Sliding of coherent twin boundaries, *Nature Comm.* 8 (2017) 1108.
- [31] Y. Yue, Q. Zhang, X. Zhang, Z. Yang, P. Yin, L. Guo, In situ observation of twin boundary sliding in single crystalline Cu nanowires, *Small* 13 (2017) 1604296.
- [32] C.R. Weinberger, A.T. Jennings, K. Kang, J.R. Greer, Atomistic simulations and continuum modeling of dislocation nucleation and strength in gold nanowires, *J. Mech. Phys. Solids* 60 (2012) 84-103.
- [33] J. Diao, K. Gall, M.L. Dunn, Yield strength asymmetry in metal nanowires, *Nano Lett.* 4 (2004) 1863-1867.
- [34] G. Sainath, B.K. Choudhary, Orientation dependent deformation behaviour of BCC iron nanowires, *Comput. Mater. Sci.* 111 (2016) 406-415.
- [35] M.A. Tschopp, D.L. McDowell, Tension-compression asymmetry in homogeneous dislocation nucleation in single crystal copper, *Appl. Phys. Lett.* 90 (2007) 121916.
- [36] I. Salehinia, D.F. Bahr, Crystal orientation effect on dislocation nucleation and multiplication in FCC single crystal under uniaxial loading, *Inter. J. Plast.* 52 (2014) 133-146.
- [37] H. Xie, T. Yu, F. Yin, Tension-compression asymmetry in homogeneous dislocation nucleation stress of single crystals Cu, Au, Ni and Ni₃Al, *Mater. Sci. Eng. A* 604 (2014) 142-147.